

Research Article

Fine defect engineering of graphene friction

Aitor Zambudio^{a, b}, Enrico Gnecco^c, Jaime Colchero^a, Rubén Pérez^{d, e},
Julio Gómez-Herrero^{b, e}, Cristina Gómez-Navarro^{b, e, *}

^a Optics and Nanophysics Research Center, Universidad de Murcia, 30100, Murcia, Spain

^b Condensed Matter Physics Dept., Universidad Autónoma de Madrid, Madrid, E-28049, Spain

^c Otto Schott Institute of Materials Research, Friedrich Schiller University of Jena, D-07743, Jena, Germany

^d Theory Condensed Matter Physics Dept., Universidad Autónoma de Madrid, Madrid, E-28049, Spain

^e Condensed Matter Physics Center, Universidad Autónoma de Madrid, Madrid, E-28049, Spain



ARTICLE INFO

Article history:

Received 18 March 2021

Received in revised form

28 May 2021

Accepted 23 June 2021

Available online 25 June 2021

Keywords:

Graphene

Friction

Vacancies

Defects

Tribology

ABSTRACT

Two-dimensional materials, in particular graphene, exhibit a low friction coefficient and good wear properties. However, the tribological properties of these materials strongly depend on faint differences at the atomic level, and the coexistence of different type of atomic defects in studied samples up to date led to experimental results difficult to reconcile. In our work, we quantified the influence of controlled-induced atomic monovacancies on the frictional behaviour of graphene. Less than 0.1% of atomic vacancies induced a fivefold increase in the effective friction coefficient. We showed that friction force microscopy resolved monoatomic vacancies and provided the real-space distribution of their influence on the tribology of graphene. Two factors contributed to this increment in friction: one was related to enhanced reactivity of dangling bonds localized at the monovacancy ($\sim 1 \text{ nm}^2$), that accounted for $\sim 20\%$ of the increase; and a more extended one ($\sim 25 \text{ nm}^2$) arose from the long-range strain distribution around these defects, characteristic of graphene. These results unveil the subtle connection between friction, reactivity, and mechanical properties in two-dimensional materials.

© 2021 The Author(s). Published by Elsevier Ltd. This is an open access article under the CC BY-NC-ND license (<http://creativecommons.org/licenses/by-nc-nd/4.0/>).

1. Introduction

Friction has a deep influence in our daily life. It dictates durability, energy efficiency and thus environmental impact of any moving mechanical assembly. In order to minimize the adverse effects of energy loss in frictional processes, lubricants are used. For decades, graphite has been employed as a solid lubricant or as additive in liquid lubricants [1,2]. More recently graphene, a single layer of graphite, has been shown to preserve the low wear properties of its three-dimensional (3D) counterpart [3,4]. Moreover, it shows chemical inertness, thermal stability, extreme strength, and high flexibility. These features make graphene a promising material as a multifunctional and active part of nanoscale devices; such as electromechanical systems [5], molecular motors [6], or triboelectric nanogenerators [7]. Here, energy dissipation through nanomechanical contact plays a major role.

Graphene and other two-dimensional (2D) materials provide a

unique platform for fundamental tribological investigations [8]–[10]. The extreme out-of-plane flexibility of these atomic thin materials has a substantial impact on their frictional behaviour, and differentiates them from conventional 3D materials [3]. For instance, 2D materials, if slid by an Atomic Force Microscopy (AFM) tip, pucker up and snap at the tip. This increases the contact area and effective friction [11]. Besides, unique effects in lateral corrugation of atomic thin materials are due to high flexibility [12] and influence their tribological response.

Graphene presents a variety of frictional behaviours because of subtle structural characteristics caused by different preparation methods or post-processing procedures. In this context, the controlled modification of the graphene atomic lattice emerges as a way to tune friction, at the same time posing key questions on the relationship between the tribology and the atomic structure of this material. Different studies revealed the friction properties of fluorinated [13,14], oxidized [15,16], and hydrogenated [17,18] graphene. These works agree that defects and chemical functionalization of graphene result in increased friction, but they differ in the mechanisms used to address this observation. For example, some authors [15] attribute the increase in friction to

* Corresponding author. Condensed Matter Physics Dept., Universidad Autónoma de Madrid, Madrid, E-28049, Spain.

E-mail address: cristina.gomez@uam.es (C. Gómez-Navarro).

enhanced out-of-plane flexibility near multiatomic vacancies; others instead [17] assess that the enhanced friction is due to the reactivity of the dangling bonds at the edges of multiatomic vacancies.

Therefore, current efforts are now directed towards identifying the mechanisms and fundamental length scales responsible for changes in friction in 2D materials upon defect presence. Surprisingly, few works report on the friction of single atomic vacancies. This type of defect is the simplest and most common structural modification in as-grown graphene [19]; hence, it is a good starting point to understand its tribology.

In our work, we prepared graphene with a well-defined gradient of atomic vacancies by argon ions bombardment. Using AFM, we measured friction maps that allowed us to determine changes in the friction coefficient with nanometric precision. At the atomic scale, these maps exhibited the characteristic stick-slip behaviour of the atomic lattice and a pronounced friction peak of 1 nm in size at the vacancies. This agrees with atomistic simulations based on the Prandtl-Tomlinson model. Importantly, we found that about 80% of the increase in friction originated from larger regions (25 nm²) around the atomic defects. This made these regions the

main contributors to the observed high impact of atomic monovacancies on friction properties at the mesoscale. The remaining 20% was highly localized on the defect. Combining both effects, we found that just 0.06% of atomic vacancies yielded a fivefold increase of the effective friction coefficient.

2. Materials and methods

Fig. 1 illustrates the key elements of our work. Graphene was obtained by micromechanical exfoliation of graphite. This procedure ensures an initial extremely low density of defects. Fig. 1a shows an optical image of a graphene flake on a SiO₂ (300 nm)/Si substrate. The number of layers of graphene flakes was determined from Raman spectra, as reported by Ferrari and colleagues in 2006 [20]. The flake in Fig. 1 presented increasing thickness from one to four monolayers of graphene. A selected region of this flake was irradiated with 140 eV Ar⁺ using a movable mask and several controlled irradiation steps, as described in more detail in the Supporting Info (S11). This method generates a random distribution of defects, whose density uniformly decays from left to right. Fig. 1b depicts the variation in the density of defects, that goes from a

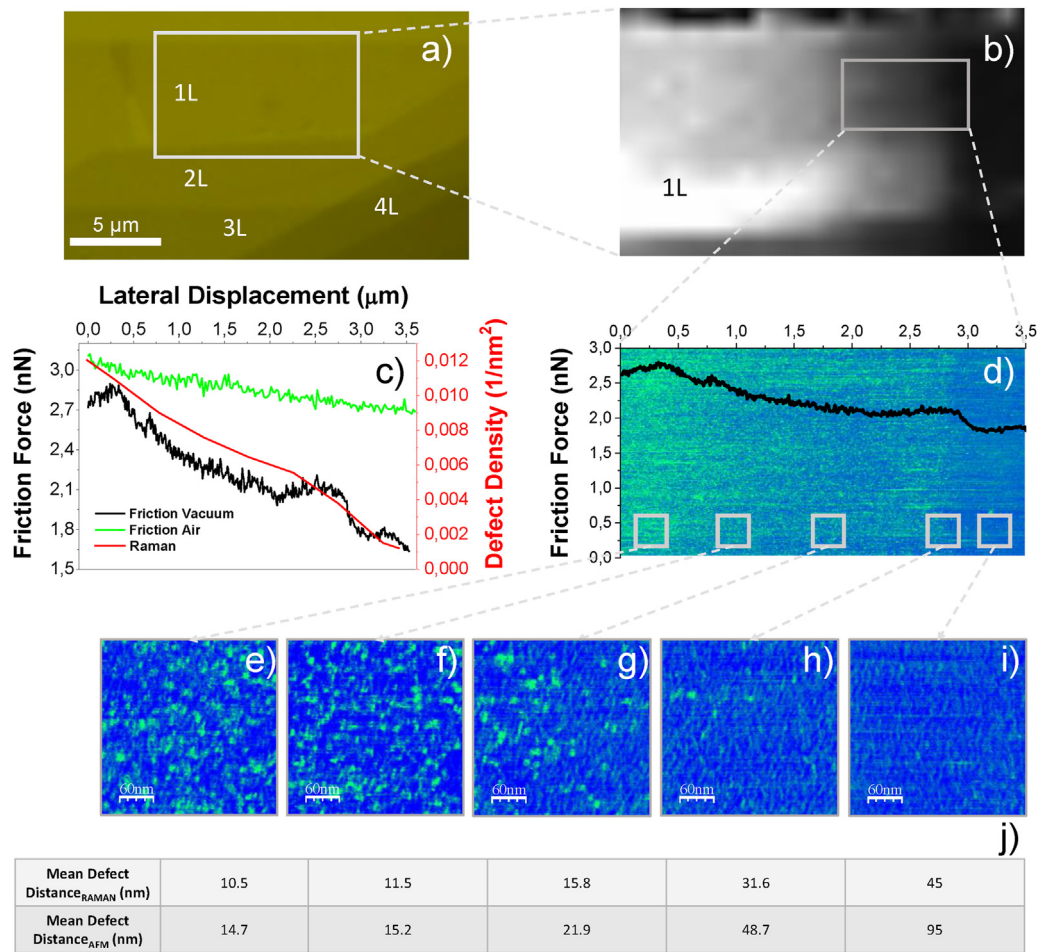


Fig. 1. a) Optical image (22 × 14 μm) of a graphene flake on a SiO₂ (300 nm)/Si substrate containing regions with 1, 2, 3, and 4 layers as depicted in the image. b) Micro-Raman image showing the I_D/I_G relation acquired on the marked region of panel a) after irradiation. The contrast quantifies the monovacancy density in the sample. The mean defect distance in the left part of the image corresponds to 7 nm. c) RED: defect density vs. X position data in the region marked in panel b. In this image, the mean defect distance in the left part of the white rectangle corresponds to 9 nm. BLACK AND GREEN: friction force vs. X position acquired in air ambient conditions (green) and vacuum (black). This trend was robust over a large range of experimental conditions (forces from 0.1 nN to 20 nN; different probes, scan velocities, and samples). d) Lateral force image acquired in the marked region of panel b applying a normal force of 1 nN. The inset represents the average friction force along the vertical direction of this image acquired in high vacuum (black). e) to i) Zoom-in lateral force images of the regions marked in panel d), where e) corresponds to the region with the highest density of vacancies and i) to the pristine region. j) Mean distance between defects extracted from Raman spectra (upper row) and friction force microscopy images (lower row). (A colour version of this figure can be viewed online.)

minimum of less than $1000 \text{ defects}/\mu\text{m}^2$ (“pristine”), to a maximum of $20,000 \text{ defects}/\mu\text{m}^2$. Such densities correspond to a mean distance between defects of more than 30 nm and of $\approx 7 \text{ nm}$, respectively. The type and density of the defects were characterized by Raman spectroscopy, as reported in Refs. [21,22]. Specifically, the density of the defects was estimated from the ratio between D and G peaks, as described in by Cançado et al. [22]. The nature of the defects was characterized using the intensity ratio between D and D' peaks. In our samples, this ratio was around 8, indicating sp^2 character, according to Eckmann et al. [21]. Additionally, we used Scanning Tunnelling Microscopy (STM) on graphite samples in ambient conditions to characterize the defects created in the same conditions as those used for our samples (see SI2). In these images, defects appeared as those obtained for single vacancies in graphene in ultra-high vacuum (UHV) conditions [23], in agreement with first principle simulations of single vacancies [24]. We obtained the same results on the density and sp^2 -point-like character of the defects with both techniques.

To characterize the nanotribological behaviour, we investigated our samples after irradiation using AFM, to acquire surface topography and friction images. Contact mode AFM images were performed with MikroMasch HQ: CSC38/Al BS silicon probes with a nominal spring constant of 0.03 N/m and a tip radius of $6\text{--}8 \text{ nm}$. Each probe was individually calibrated as described in SI3. Simultaneous topography and friction images were taken at 1 nN of applied normal force (F_n).

First, we characterized the sample in ambient conditions, observing that the friction force increased with an increasing density of vacancies, as depicted in Fig. 1c. Since tribological properties of surfaces, and particularly of graphene, are dictated by adsorbed molecules [18], subsequent measurements were acquired in a high vacuum chamber ($4 \times 10^{-6} \text{ mbar}$), always keeping the sample temperature higher than 60°C . These conditions avoid physisorption and spurious sources of friction [18]. Samples were also scanned at a high loading force ($F_n > 30 \text{ nN}$) before friction measurements, to remove larger adsorbates from the surface as

reported in Ref. [18]. Under these controlled conditions, we observed that the friction force increases with an increasing density of vacancies in a more pronounced manner in comparison to ambient measurements, as displayed in Fig. 1c.

3. Results

We obtained $300 \times 300 \text{ nm}$ images at several locations along the X-axis (with different vacancy densities) as those shown in Fig. 1e–i. This allowed us to resolve well-defined features corresponding to patches of $3\text{--}6 \text{ nm}$ in lateral size and $3\text{--}6 \text{ nN}$ of lateral force (at 1 nN of applied normal force). These patches were more densely packed in the regions with a higher density of vacancies, as determined from the Raman spectra; therefore, we concluded that they correspond to defects. Remarkably, the density of these patches of increased friction coincided with the estimation of the density of monovacancies based on the well-established relation between the peaks intensity in Raman spectra [22], as illustrated in Fig. 1j. It was therefore plausible to assign each friction patch of $3\text{--}6 \text{ nm}$ in size with a single carbon vacancy.

These vacancies could also be imaged in nanometre-sized images; hence we selected an area with a diluted density of defects to carry out small size images. Fig. 2a shows one of these images on pristine graphene. In non-defective areas, a regular pattern with an average lateral force of $\sim 1 \text{ nN}$ (applied load of 1 nN) revealed characteristic ordered stick-slip events at the atomic scale [25]. Similar images on defective areas showed regions with longer ($>1 \text{ nm}$) stick phases reaching lateral forces up to $\sim 5 \text{ nN}$. A representative lateral force map covering a single defect is shown in Fig. 2b. Applying the Prandtl-Tomlinson model for atomic-scale friction reproduced these features. In line with previous works [26], as detailed in SI4, we considered a spring-coupled point mass sliding over a surface, mediated by a suitable interaction potential. Here, pristine graphene was modelled by a hexagonal pattern of sinusoidal potential wells with amplitude U_G . A deep Gaussian potential well (depth U_1 and width σ) was then superimposed to

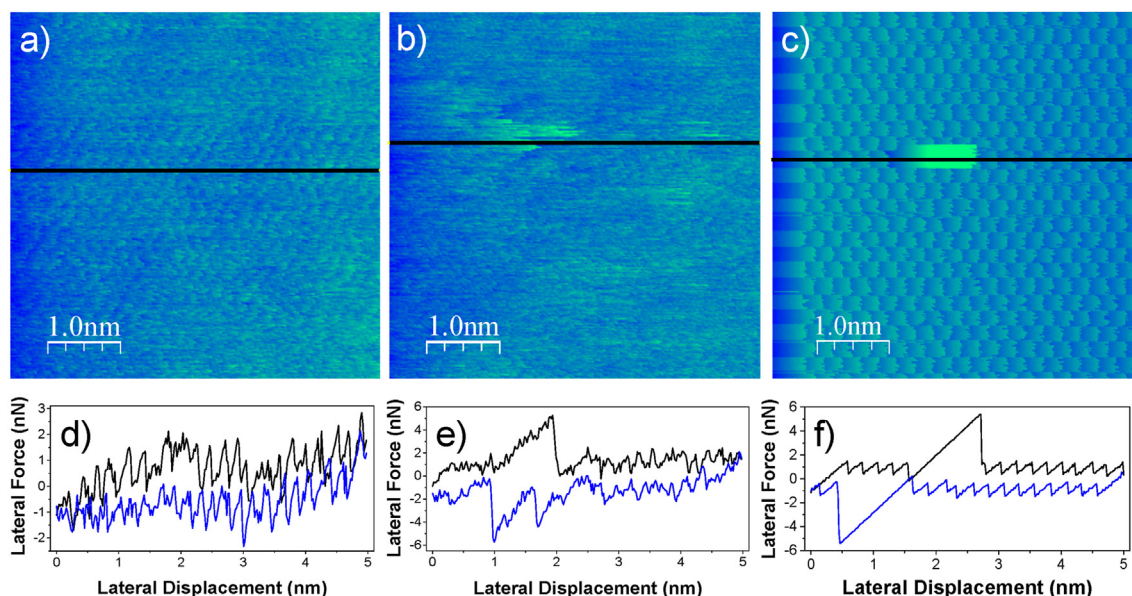


Fig. 2. a) Measured lateral force image of a pristine region of the flake showing stick-slip features. b) Lateral force image of a region of the flake with defects. We can observe the stick-increased feature of the defect, as well as the regular stick-slip behaviour of graphene lattice. c) Lateral force image obtained from the Prandtl-Tomlinson model. d) to f) Profiles below each image correspond to the black lines in the upper images (acquired from left to right) and a simultaneous one on the analogous image acquired from right to left. Simulated friction maps corresponding to the parameter values $U_G = 0.4 \text{ eV}$, $U_1 = 3 \text{ eV}$, $k = 5 \text{ N/m}$, $v = 25 \text{ nm/s}$, and $T = 300 \text{ K}$. The surface lattice has also been rotated by an angle of 40° with respect to the main crystallographic directions. (A colour version of this figure can be viewed online.)

this graphene template in the position of a carbon atom to simulate a vacancy:

$$U_{hole} = -U_1 \exp\left[\frac{-x^2 + y^2}{2\sigma^2}\right] \quad (1)$$

This choice was dictated by the fact that the precise structure of the tip apex used in the experiment is unknown. The parameter values have been consequently tuned to the results obtained in the AFM measurements.

As shown by Socoliuc et al. [27], the amplitude U_G can be estimated from the maximum of the measured lateral force ($F_G \approx 1.5$ nN) as $U_G = aF_G/(2\pi) \approx 0.4$ eV, where $a = 0.246$ nm is the lattice constant. For the effective spring constant, the value $k = 5$ N/m is used, as given by the slopes of the stick phases in the cross-section in Fig. 2d. For the width of the Gaussian profile, we chose the value $\sigma = a/6$, assuming that the energy landscape was not perturbed on distances larger than a . With this assumption, commonly used in conventional materials, a peak value of the friction force $F_1 \approx 5$ nN

(similar to those measured on a vacancy) was found for a value $U_1 \approx 3$ eV of the potential depth. The corresponding friction map, as obtained by solving the Langevin equation at temperature $T = 300$ K with the Ermak algorithm [26], is shown in Fig. 2c. Both width and length of the “high friction strip” originated from the potential well (1.3 nm and 0.4 nm, respectively) are consistent with those of the analogous experimental feature observed in Fig. 2b.

To further quantify frictional behaviour, we also acquired friction images while sweeping the loading force (F_n). The corresponding data set $F_{fric}(x,y, F_n)$ is visualized in a 3D plot in Fig. 3a. We used real-time and post-data acquisition algorithms in order to precisely align individual images $F_{fric}(x,y)$ to study the variation of friction with loading force for specific locations on the sample surface. We obtained nanometric resolution and improved data dispersion, as compared to single images. From these data, we concluded that, for positive F_n , the $F_{fric}(F_n)$ dependence can be described in a very good approximation by a linear relation. This allowed us to assign an effective friction coefficient μ_{eff} to each

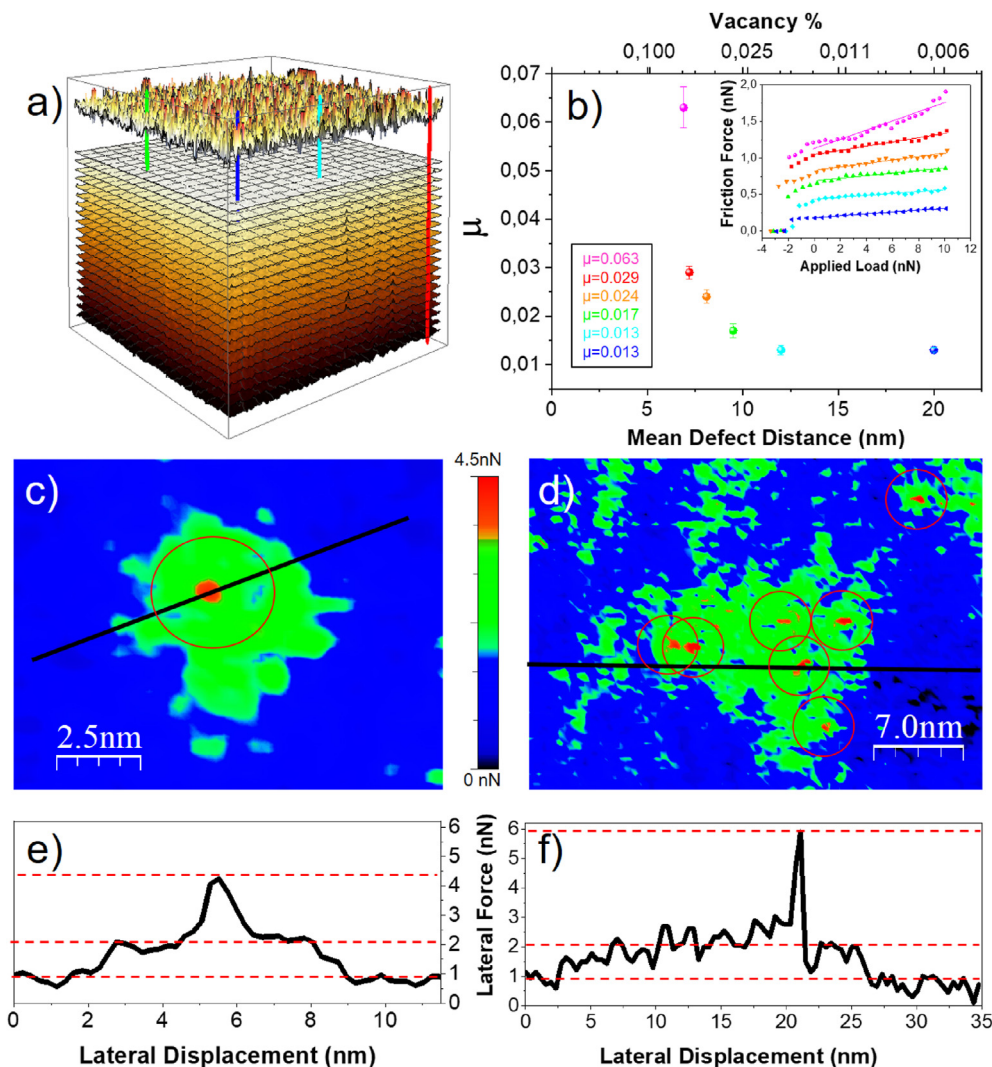


Fig. 3. a) 3D dataset $F_{fric}(x,y, F_n)$ acquired at a region of 400–400 nm, with a mean defect distance of 7.5 nm. The four coloured vertical lines correspond to the dataset at a constant position (x_0, y_0) and variable loading force F_n . The top image corresponds to the friction coefficient calculated as the slope of F_{fric} vs. F_n of every (x,y) position. b) COLOURED POINTS: Effective friction coefficient, μ_{eff} , for 500–500 nm regions, as a function of the mean distance between vacancies extracted from the Raman spectrum. The ratio between the pink and blue points is 4.9, indicating a ≈ 5 -fold increase in friction from pristine graphene, in comparison to that with an average distance between vacancies of 7 nm. INSET: Friction force vs Applied load for the same regions as the main panel, with colour correspondence. c) Coloured map of the friction measured in a region with an isolated vacancy, where the localized friction peak is shown in red, and the surrounding increased friction area is depicted in green. d) Coloured map of the friction measured in a region with several vacancies. e) and f) Friction profiles along the black lines shown in images c) and d), respectively. (A colour version of this figure can be viewed online.)

image point. Representative F_{fric} (F_n) curves are illustrated in the inset of Fig. 3b.

We quantified the effect of atomic vacancies on the tribological properties of graphene at the mesoscale by averaging the friction coefficient, μ_{eff} , for a complete 500·500 nm region, where the density of defects was nearly constant. Then, we plotted it as a function of the mean distance between defects. As a result, μ_{eff} increased with the density of vacancies, from 0.013 up to 0.063, as illustrated in Fig. 3b. Graphene showed a fivefold increase in the effective friction coefficient.

In addition to the mesoscale friction coefficient (μ_{eff}) in 500·500 nm areas, we were able to compute the friction coefficient associated with regions $<1 \text{ nm}^2$, where the single vacancies are located. Here, we found a value of $\mu_{\text{DEF}} = 0.23$, as discussed in SI5. Considering that the vacancy density is below 0.1%, this value is not large enough to justify the fivefold increase in μ_{eff} measured at the micron scale. Further analysis of the images revealed that vacancies also led to a more extended contribution (25 nm^2) in the areas around them, in addition to the localized friction peak at the vacancy position. This caused an increase in friction, although three times lower than that of the peaks localized at the vacancies. As seen in Fig. 3c, the very localized ($<1 \text{ nm}^2$) friction peaks were always accompanied by a smaller increase of lateral force in their surrounding area, that expanded up to 5 nm in radius. This representative image shows an isolated vacancy, where the red spot corresponds to the localized friction peak at the vacancy position, and the surrounding green area represents a smaller ($\sim 1/3$) friction increase. On a slightly larger scale, the friction image in Fig. 3d shows a 900 nm^2 area with a higher density of defects, where the areas influenced by the vacancies nearly overlapped in some regions.

To discern the contribution of each of these features to the global friction, we computed μ_{eff} for 500·500 nm regions, excluding the areas with localized friction peaks. We found that these values closely approached those of the global friction coefficient. Indeed, these highly localized friction peaks at the vacancy

position represented between 5 and 25% of the global friction for our defect densities. These regions with approximately 5 nm of radius around the defects, and not the more localized pronounced peaks observed at the vacancies site, were the main cause for the observed increase in μ_{eff} .

Two different aspects contributed to a global friction enhancement: (i) the localized (1 nm^2) friction enhancement at the monovacancies, and (ii) the effect acting on larger regions (25 nm^2) surrounding the vacancies. We believe that the former effect is due to the chemical reactivity of the dangling bonds [17] at the vacancy site. The strong sp^2 character of our vacancies, as revealed by Raman spectroscopy and STM images, implied the presence of dangling bonds in the vicinity of the missing atom. Molecular Dynamic simulations of sliding tips on monoatomic [19] and multia-atomic [17] vacancies in graphene have revealed a friction increase due to enhanced interaction between the tip and the surface at the vacancy site. The second effect can be explained by the fact that friction in two-dimensional materials is strongly influenced by the great out-of-plane flexibility of these materials. Recent Molecular Dynamic simulations [28] and large-scale ab initio calculations [29] have shown that single-atom vacancies create a threefold symmetry stress distribution around them. This distribution expands around 3 nm from the missing C atom and survives even in the presence of a global strain. In these areas, tensile and compressive stress alternate. Fig. 4a depicts an in-plane strain map calculated by Molecular Dynamics of the region surrounding one monovacancy as reported in Ref. [28]. The maximum tensile stress observed around vacancies is $\sim 2.15 \text{ N/m}$, which corresponds to a local strain increase of 0.65%. This high stress slowly decays with the distance to the vacancy, reaching lengths of 3–5 nm from the carbon-missing atom. To compare with our friction images, we have superimposed one of these 2D stress maps with our results (Fig. 4c), using the same scale bar. Here, we illustrate how these two maps show similar lengths.

This stress pattern has been shown to have important consequences on the large-scale properties of graphene, like its thermal

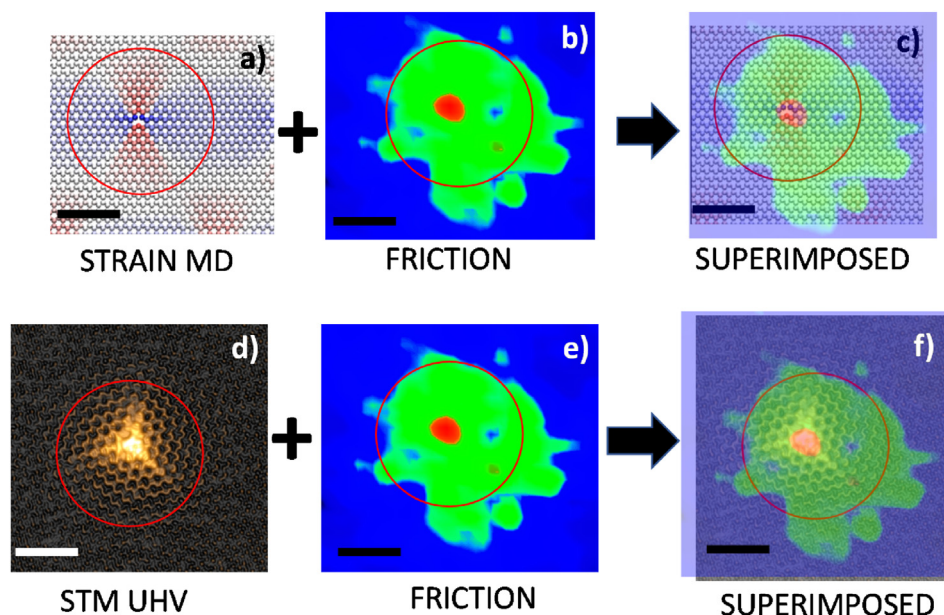


Fig. 4. The scale bar for all images is 2 nm. Red circles are 2.5 nm in radius. a) 2D stress map obtained from Molecular Dynamic simulations in Ref. [28] in a region surrounding a carbon monovacancy. b) and e) Lateral force images centred on a carbon monovacancy. c) Superposition of panels a) and b). d) Experimental STM image of a carbon monovacancy acquired in UHV conditions. (courtesy of I. Brihuega) f) Superposition of panels d) and e). Both c) and f) panels show a clear spatial correlation between the defect influence area on friction images acquired in the present work and previous theoretical and experimental results on similar graphene monovacancies. (A colour version of this figure can be viewed online.)

expansion coefficient [28]. In the case of friction, stress fields are known to modulate the local pinning capability of the contact interface, favouring the puckering effect [3]. It has also been reported that in-plane straining strongly modulates friction in graphene by changing the atomic contact quality of the sliding interface [30,31]. These alternating areas of tensile and compressive strain around the vacancies can provide extra flexibility to the contact and lead to increased friction in the areas around the defects. The proper validation of this subtle dynamical effect for a sliding tip would require extremely long simulation times [28], that would be well beyond the state-of-the-art in the field. Nevertheless, this mechanism provides a plausible explanation to our experimental observations with proper length scales. It also justifies the high efficiency of vacancies in increasing friction coefficient when compared with sp^3 modification, such as fluorination [13,14], where this long-range effect is absent.

Additionally, different phenomena have been described to show a long-range effect in defective graphene. The electronic effect of a carbon missing atom decays as r^2 and reaches regions more than 3 nm away from the position of the missing atom. STM images of carbon monovacancies and friction maps are superimposed in Fig. 4f to illustrate this effect.

4. Conclusions

In this work, we established robust structure-property relationships through μ_{eff} for graphene with atomic vacancies. We identified these defects with friction force microscopy and provided the real-space distribution of their influence on the tribology of graphene. Our data indicates that other mechanisms, different from the typical enhanced reactivity associated with these defects, have a major contribution to friction. We suggest that the strain distribution surrounding the vacancies, linked to the 2D nature of graphene, can account for the results presented above. The fundamental aspects of the tribology of graphene revealed in the present work could be extended to other two-dimensional materials, allowing a fine-tuning and understanding of their friction properties.

Notes

The authors declare no conflict of interest.

Credit author statement

A Z performed the experiments, analysed and contributed to the interpretation of experimental results.

J C developed data processing and contributed to the interpretation of experimental results.

E G performed the analysis based on the Prandtl-Tomlinson model.

R P contributed to the interpretation of the experimental results and the friction mechanisms.

J G-H contributed to the design and implementation of the experiments, aided in interpreting the results and worked on the manuscript.

C G-N conceived and designed the experiments, aided in interpreting the results and wrote the paper with input from all authors.

All authors participated in joint discussions and the writing of the manuscript.

Declaration of competing interest

The authors declare that they have no known competing financial interests or personal relationships that could have

appeared to influence the work reported in this paper.

Acknowledgements

We acknowledge M M Ugeda and I Brihuega for the STM image of Fig. 4d. We acknowledge financial support from Spanish MINECO (projects PID2019-106268GB-C31, PID2019-104272RB-C52, ENE2016-79282-C5-4, and MAT2017-83273-R); Comunidad de Madrid (S2018/NMT-4511, NMAT, 2D-CM); and Ramon Areces Foundation. RP, JG-H, and CG-N acknowledge support from the Spanish Ministry of Science and Innovation, through the “María de Maeztu” Programme for Units of Excellence in R&D (CEX2018-000805-M).

Appendix A. Supplementary data

Supplementary data to this article can be found online at <https://doi.org/10.1016/j.carbon.2021.06.064>.

References

- [1] B. Jin, G. Chen, J. Zhao, Y. He, Y. Huang, J. Luo, Improvement of the lubrication properties of grease with Mn3O4/graphene (Mn3O4#G) nanocomposite additive, *Friction* (2020), <https://doi.org/10.1007/s40544-020-0412-1>.
- [2] B. Jin, J. Zhao, G. Chen, Y. He, Y. Huang, J. Luo, In situ synthesis of Mn3O4/graphene nanocomposite and its application as a lubrication additive at high temperatures, *Appl. Surf. Sci.* 546 (2021) 149019, <https://doi.org/10.1016/j.apsusc.2021.149019>.
- [3] C. Lee, Q. Li, W. Kalb, X.Z. Liu, H. Berger, R.W. Carpick, J. Hone, Frictional characteristics of atomically thin sheets, *Science* 328 (2010) 76–80, <https://doi.org/10.1126/science.1184167>.
- [4] D. Berman, A. Erdemir, A.V. Sumant, Graphene: a new emerging lubricant, *Mater. Today* 17 (2014) 31–42, <https://doi.org/10.1016/j.mattod.2013.12.003>.
- [5] Changyao Chen, J. Hone, Graphene nanoelectromechanical systems, *Proc. IEEE* 101 (2013) 1766–1779, <https://doi.org/10.1109/JPROC.2013.2253291>.
- [6] O. Akhavan, M. Saadati, M. Jannesari, Graphene jet nanomotors in remote controllable self-propulsion swimmers in pure water, *Nano Lett.* 16 (2016) 5619–5630, <https://doi.org/10.1021/acs.nanolett.6b02175>.
- [7] S. Kim, M.K. Gupta, K.Y. Lee, A. Sohn, T.Y. Kim, K.-S. Shin, D. Kim, S.K. Kim, K.H. Lee, H.-J. Shin, D.-W. Kim, S.-W. Kim, Transparent flexible graphene triboelectric nanogenerators, *Adv. Mater.* 26 (2014) 3918–3925, <https://doi.org/10.1002/adma.201400172>.
- [8] J.-H. Ko, S. Kwon, I.-S. Byun, J.S. Choi, B.H. Park, Y.-H. Kim, J.Y. Park, Nano-tribological properties of fluorinated, hydrogenated, and oxidized graphenes, *Tribol. Lett.* 50 (2013) 137–144, <https://doi.org/10.1007/s11249-012-0099-1>.
- [9] D. Berman, A. Erdemir, A.V. Sumant, Approaches for achieving superlubricity in two-dimensional materials, *ACS Nano* 12 (2018) 2122–2137, <https://doi.org/10.1021/acs.nano.7b09046>.
- [10] M.R. Vazirisereshk, A. Martini, D.A. Strubbe, M.Z. Baykara, Solid lubrication with MoS₂: a review, *Lubricants* 7 (2019) 57, <https://doi.org/10.3390/lubricants7070057>.
- [11] S. Li, Q. Li, R.W. Carpick, P. Gumbsch, X.Z. Liu, X. Ding, J. Sun, J. Li, The evolving quality of frictional contact with graphene, *Nature* 539 (2016) 541–545, <https://doi.org/10.1038/nature20135>.
- [12] A. Smolyanitsky, J.P. Killgore, Anomalous friction in suspended graphene, *Phys. Rev. B* 86 (2012) 125432, <https://doi.org/10.1103/PhysRevB.86.125432>.
- [13] Q. Li, X.-Z. Liu, S.-P. Kim, V.B. Shenoy, P.E. Sheehan, J.T. Robinson, R.W. Carpick, Fluorination of graphene enhances friction due to increased corrugation, *Nano Lett.* 14 (2014) 5212–5217, <https://doi.org/10.1021/nl502147t>.
- [14] S. Kwon, J.-H. Ko, K.-J. Jeon, Y.-H. Kim, J.Y. Park, Enhanced nanoscale friction on fluorinated graphene, *Nano Lett.* 12 (2012) 6043–6048, <https://doi.org/10.1021/nl204019k>.
- [15] P. Gajurel, M. Kim, Q. Wang, W. Dai, H. Liu, C. Cen, Vacancy-controlled contact friction in graphene, *Adv. Funct. Mater.* 27 (2017) 1702832, <https://doi.org/10.1002/adfm.2017702832>.
- [16] X. Zeng, Y. Peng, H. Lang, L. Liu, Controllable nanotribological properties of graphene nanosheets, *Sci. Rep.* 7 (2017) 41891, <https://doi.org/10.1038/srep41891>.
- [17] J. Liu, Y. Qi, Q. Li, T. Duan, W. Yue, A. Vadakkepatt, C. Ye, Y. Dong, Vacancy-controlled friction on 2D materials: roughness, flexibility, and chemical reactions, *Carbon* 142 (2019) 363–372, <https://doi.org/10.1016/j.carbon.2018.10.048>.
- [18] G. Fessler, B. Eren, U. Gysin, T. Glatzel, E. Meyer, Friction force microscopy studies on SiO₂ supported pristine and hydrogenated graphene, *Appl. Phys. Lett.* 104 (2014), 041910, <https://doi.org/10.1063/1.4863832>.
- [19] H. Pang, H. Wang, M. Li, C. Gao, Atomic-scale friction on monovacancy-defective graphene and single-layer molybdenum-disulfide by numerical analysis, *Nanomaterials* 10 (2020) 87, <https://doi.org/10.3390/nano10010087>.

- [20] A.C. Ferrari, J.C. Meyer, V. Scardaci, C. Casiraghi, M. Lazzeri, F. Mauri, S. Piscanec, D. Jiang, K.S. Novoselov, S. Roth, A.K. Geim, Raman spectrum of graphene and graphene layers, *Phys. Rev. Lett.* 97 (2006) 187401, <https://doi.org/10.1103/PhysRevLett.97.187401>.
- [21] A. Eckmann, A. Felten, A. Mishchenko, L. Britnell, R. Krupke, K.S. Novoselov, C. Casiraghi, Probing the nature of defects in graphene by Raman spectroscopy, *Nano Lett.* 12 (2012) 3925–3930, <https://doi.org/10.1021/nl300901a>.
- [22] L.G. Cançado, A. Jorio, E.H.M. Ferreira, F. Stavale, C.A. Achete, R.B. Capaz, M.V.O. Moutinho, A. Lombardo, T.S. Kulmala, A.C. Ferrari, Quantifying defects in graphene via Raman spectroscopy at different excitation energies, *Nano Lett.* 11 (2011) 3190–3196, <https://doi.org/10.1021/nl201432g>.
- [23] M.M. Ugeda, I. Brihuega, F. Guinea, J.M. Gómez-Rodríguez, Missing atom as a source of carbon magnetism, *Phys. Rev. Lett.* 104 (2010), 096804, <https://doi.org/10.1103/PhysRevLett.104.096804>.
- [24] H.A. Mizes, J.S. Foster, Long-range electronic perturbations caused by defects using scanning tunneling microscopy, *Science* 244 (1989) 559–562, <https://doi.org/10.1126/science.244.4904.559>.
- [25] E. Gnecco, E. Meyer, *Fundamentals of Friction and Wear on the Nanoscale*, Springer International Publishing, Switzerland, 2015. <https://www.springer.com/gp/book/9783319105598>.
- [26] P. Steiner, R. Roth, E. Gnecco, A. Baratoff, S. Maier, T. Glatzel, E. Meyer, Two-dimensional simulation of superlubricity on NaCl and highly oriented pyrolytic graphite, *Phys. Rev. B* 79 (2009), 045414, <https://doi.org/10.1103/PhysRevB.79.045414>.
- [27] A. Socoliuc, R. Bennewitz, E. Gnecco, E. Meyer, Transition from stick-slip to continuous sliding in atomic friction: entering a new regime of ultralow friction, *Phys. Rev. Lett.* 92 (2004) 134301, <https://doi.org/10.1103/PhysRevLett.92.134301>.
- [28] G. López-Polín, M. Ortega, J.G. Vilhena, I. Alda, J. Gomez-Herrero, P.A. Serena, C. Gomez-Navarro, R. Pérez, Tailoring the thermal expansion of graphene via controlled defect creation, *Carbon* 116 (2017) 670–677, <https://doi.org/10.1016/j.carbon.2017.02.021>.
- [29] L. Rodrigo, P. Pou, R. Pérez, Graphene monovacancies: electronic and mechanical properties from large scale ab initio simulations, *Carbon* 103 (2016) 200–208, <https://doi.org/10.1016/j.carbon.2016.02.064>.
- [30] S. Zhang, Y. Hou, S. Li, L. Liu, Z. Zhang, X.-Q. Feng, Q. Li, Tuning friction to a superlubric state via in-plane straining, *Proc. Natl. Acad. Sci. Unit. States Am.* 116 (2019) 24452–24456, <https://doi.org/10.1073/pnas.1907947116>.
- [31] K. Wang, W. Ouyang, W. Cao, M. Ma, Q. Zheng, Robust superlubricity by strain engineering, *Nanoscale* 11 (2019) 2186–2193, <https://doi.org/10.1039/C8NR07963C>.